

## Numerical Investigation of Coaxial Turbulent Jet

NABIL BELKACEM SAFER<sup>1†</sup>, ABDELHADI. BEGHIDJA<sup>2</sup>

<sup>1</sup> Department of Mechanical Engineering, laboratory of Renewable energies and sustainable development

<sup>2</sup> Department of Mechanical Engineering, laboratory of Renewable energies and sustainable development  
University of Constantine  
ALGERIA  
Safer\_n@hotmail.com

*Abstract:* - Implantation of the 3D compressible parallel code to study a compressible turbulent coaxial jet at higher number of Reynolds. The model of large eddy simulation used. In this model, only the larger structures are computed, and the effects of smaller scales are taken into account via a sub-grid scale model. The code was parallelized using the Message Passing Interface (MPI) library. The resolution full Navier Stokes equations are based on the compute the fluxes. In order to compute the fluxes, the fluxes were split into viscous fluxes and convective fluxes. Viscous fluxes are computed from the second order central differences in space. The convective fluxes are evaluated using the approximate Riemann solver. Approximate Riemann solver based on the linearization of the differential relations along the characteristic curves of the one-dimensional hyperbolic conservation laws. The solution was advanced in time using a two-stage explicit McCormack time-marching method, this method is accurate, efficient and simple to implement on parallel computers. The mean flow field and turbulence intensities of the coaxial jet have been calculated and analyzed. The results obtained in our simulation are found to be in very good agreement with the available experimental data of coaxial jet at similar flow conditions.

*Key-Words:* - Coaxial jet, Large Eddy Simulation, Riemann solver, MUSCL

Coaxial jets are present in various industrial devices: they effectively provide an effective means of mixing species for combustion applications. They are also used in aero-acoustics. The noise produced by a single jet can indeed be reduced through the addition of a coaxial surrounding flux. There are two types of coaxial jets: those where the velocity of the primary jet is greater than the velocity of the secondary and those where the velocity of the primary jet is lower than the velocity of the secondary jet. The coaxial jet is defined by many initial parameters, such as the primary jet expansion rate and its temperature, the secondary jet expansion rate and its temperature, the ratio of the velocities between the secondary and the primary jet. As well as the ratio between the diameters of the secondary and primary stream. Experimental work of Ko and Kwan [1] distinguished the development of the jets in three zones: the initial region, the intermediate region, and the fully merged zone. The initial region is located between the nozzle, and the end of the outer

core potential. Immediately downstream is the intermediate region which ends at the reattachment point, and finally is found the fully merged zone. The work of Champagne and Wagnanski [2] showed that coaxial jets had two distinct shear layers, one forming between the primary and secondary jets, and the second between the secondary jet and the environment. Forstall and Shapiro [3], identified that the ratio of the velocity of the secondary jet and the primary jet defined by  $Ru = \frac{U_2}{U_1}$  was then the determining parameter of the coaxial jets. Later, Favre-Marinet and Camano-Schettini [4, 5] showed that this was actually the ratio of momentum fluxes,  $M = \frac{\rho_s U_s^2}{\rho_p U_p^2}$  (where  $\rho_s$  and  $\rho_p$  are the densities of the fluid from the secondary jet and the primary jet respectively. Williams et al. [6], Dosanjh et al. [7] it was concluded that the noise produced by a single jet could be substantially reduced by the addition of a low velocity annular jet. The measurements made by Kwan and Ko [8] revealed two distinct peaks corresponding to the passage of vortices from the

inner shear layer and the passage of those from the outer shear layer. They deduce from their experimental results on the mean and fluctuating velocity distributions that the structure of the coaxial jet flow could be described by considering the independent shear layers. A number of previous works have focused on the instabilities that are developing in the coaxial jets. A special case interesting is the experimental configuration by Dahm et al. [9]. Studied the interaction between the coherent structures evolving in the two shear-layers. Wicker and Eaton [10] noted that the coaxial jet developed axi-symmetric mode instability, and beyond a certain value of the Reynolds number below which the instability is sinuous. Frequencies dominates in the near field of coaxial jets have also been explored in several works Au and Ko [11], Gladnick et al. [12], and Wicker and Eaton [10]. Theirs measurements show that as in the case of simple jets, a preferential mode of jet exists beyond the core potential. Camano-Schettini [13] illustrated the presence of longitudinal vortices. Zawacki et al. [14] were the first to highlight presences of a return flow. This re-circulation region (which we will also call re-circulation bubble) exists for quite high velocity ratios. According to Rehab and al. [15], the value of  $Ru_c$  seems to be between 5 and 8, depending on the shape of the injector. Rehab [16] was also interested in the behavior of this bubble. In his experiments with high Reynolds number, he showed that this re-circulation bubble oscillates at a low frequency leading to a Strouhal number of the order of  $St = 0.035$ .

In comparison with the simple jets, we find much less fundamental studies informing, us on the turbulence of these flows. In this work attempts to simulate the unsteadiness of coaxial jets, and to study the evolution of coherent structures, this is one of the objectives in this work. This nevertheless takes place in the case of monophasic coaxial jets, and velocity of the primary jet is greater than that of the secondary jet, using the model Large Eddy Simulations (LES).

## 2 Governing Equation

The full Navier–Stokes equations for two-dimensional fluid motion are written in conservative form. In Cartesian coordinates, we have:

$$\frac{\partial U}{\partial t} + \frac{\partial F}{\partial x} + \frac{\partial G}{\partial y} + \frac{\partial H}{\partial z} = 0 \tag{1}$$

Where

$$U \begin{bmatrix} \rho \\ \rho u \\ \rho v \\ \rho w \\ \rho e \end{bmatrix}$$

Where  $\rho, u, v, w$  and  $e$  are the density, the axial, radial, tangential velocity components, and the total specific energy, respectively. System (1) is completed by the definition of the total specific energy for a perfect gas:

$$\rho e = \frac{p}{\gamma - 1} + \frac{1}{2} \rho (u^2 + v^2 + w^2) \tag{2}$$

The systems of equations are closed using the equation of state for a perfect gas:

$$P = \rho RT \tag{3}$$

Spatial derivatives of fluxes in Eq. (1) for Cartesian grid can be expressed by spatial finite differencing operators that retain conservation property:

$$L_h(\bar{U}_{ijk}^n) = \frac{F_{i-\frac{1}{2},j,k}^n - F_{i+\frac{1}{2},j,k}^n}{\Delta x} + \frac{G_{i,j-\frac{1}{2},k}^n - G_{i,j+\frac{1}{2},k}^n}{\Delta y} + \frac{H_{i,j,k-\frac{1}{2}}^n - H_{i,j,k+\frac{1}{2}}^n}{\Delta z} \tag{4}$$

In order to compute the fluxes (matrices  $F, G, H$  in Eq. (1), the fluxes were split into viscous fluxes  $F_{vis}, G_{vis}$  and  $H_{vis}$  and convective fluxes  $F_{inv}, G_{inv}$ , and  $H_{inv}$ .

$$F_{inv} \begin{bmatrix} \rho u \\ p + \rho u^2 \\ \rho uv \\ \rho uw \\ (\rho e + p)u \end{bmatrix} \quad G_{inv} \begin{bmatrix} \rho v \\ \rho uv \\ p + \rho v^2 \\ \rho vw \\ (\rho e + p)v \end{bmatrix} \quad H_{inv} \begin{bmatrix} \rho w \\ \rho wu \\ \rho wv \\ p + \rho w^2 \\ (\rho e + p)w \end{bmatrix}$$

$$F_{vis} \begin{bmatrix} 0 \\ \tau_{11} \\ \tau_{12} \\ \tau_{13} \\ u\tau_{11} + v\tau_{12} + w\tau_{13} \end{bmatrix} \quad G_{vis} \begin{bmatrix} 0 \\ \tau_{21} \\ \tau_{22} \\ \tau_{23} \\ u\tau_{21} + v\tau_{22} + w\tau_{23} \end{bmatrix} \quad F_{vis} \begin{bmatrix} 0 \\ \tau_{31} \\ \tau_{32} \\ \tau_{33} \\ u\tau_{31} + v\tau_{32} + w\tau_{33} \end{bmatrix}$$

The viscous stress tensor  $\tau_{ij}$  is defined by:

$$\tau_{ij} = 2\mu S_{ij} \quad (5)$$

Where  $\mu$  are the dynamic molecular viscosity and  $S_{ij}$  the deviator part of the deformation stress tensor given by:

$$S_{ij} = \frac{1}{2} \left( \frac{\partial u_i}{\partial x_j} + \frac{\partial u_j}{\partial x_i} - \frac{2}{3} \delta_{ij} \left( \frac{\partial u_k}{\partial x_k} \right) \right) \quad (6)$$

LES is an alternative for computing flows at higher Reynolds number. In this technique, only the larger structures are computed, and the effects of smaller scales are taken into account via a sub-grid scale model. A turbulent viscosity  $\mu_t$  ensures dissipation of the smaller unresolved structures. Basically,  $\mu$  is replaced by  $\mu + \mu_t$  in Eq. (5). Various models have been built to determine an expression of this turbulent viscosity. To keep the problem as simple as possible for aerodynamics, we choose Smagorinsky's model

$$\mu_t = \rho(C_s \Delta)^2 \sqrt{2S_{ij}S_{ij}} \quad (7)$$

Where  $C_s$  is a Smagorinsky model Parameter, and  $\Delta$  is the filter width and is defined:

$$\Delta = (\Delta_x \Delta_y \Delta_z)^{1/3} \quad (8)$$

Where  $\Delta_x, \Delta_y, \Delta_z$  are the local mesh spacing in  $x, y$  and  $z$  directions respectively.

### 2.1 boundary and initial condition

In analogy to the original profile of a single jet, we use an initial velocity profile double hyperbolic tangent, defined by the inlet Domain.

$$u(r) = \begin{cases} U_s - \frac{U_p - U_s}{2} \left[ 1 - \tanh \left[ b_p \left[ \frac{r}{R_p} - \frac{R_p}{r} \right] \right] \right] si & if \geq R_m \\ U_\infty - \frac{U_s - U_\infty}{2} \left[ 1 - \tanh \left[ b_s \left[ \frac{r}{R_s} - \frac{R_s}{r} \right] \right] \right] si & if \leq R_m \end{cases} \quad (9)$$

The initial temperature profile is determined using the relationship Crocco-Busemann, which connects the temperature at the primary velocity:

$$\frac{T}{T_p}(r) = \frac{T_\infty}{T_p} + \left[ 1 - \frac{T_\infty}{T_p} \right] \frac{U}{U_p}(r) + \frac{\gamma-1}{2} M^2 \frac{U}{U_p}(r) \left[ 1 - \frac{U}{U_p}(r) \right] \quad (10)$$

A white noise is superimposed on the initial profile of the velocity in order to favor unstable modes and simulate the small scale turbulence of the upstream flow. This noise has low amplitude of the order of 3% of the maximum input velocity. The mean velocity component in the radial and tangential direction is set to zero. Randomly generated perturbations are imposed on the radial and tangential direction at the inlet. At the top and bottom boundaries, slip conditions were prescribed. At the front and back boundaries, periodic boundary and convective boundary conditions were used at the outflow, the figure.1. Show boundary conditions.

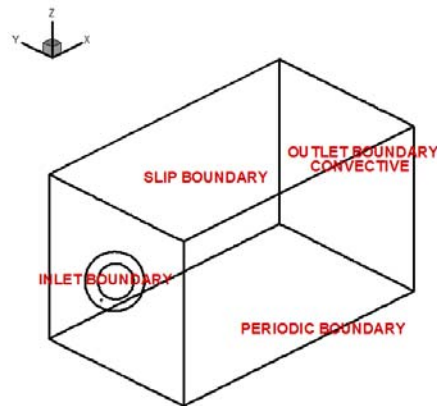


Fig.1. Boundary conditions

### 3 NUMERICAL TOOLS

The viscous fluxes are computed from the second order central difference in space. Evaluation of the convectives fluxes is done by solving a split multidimensional problem of Euler, using the approximate Riemann solver. A novel approximate linearized characteristic Riemann solver based on the linearization of the differential relations along the characteristic curves of the one-dimensional hyperbolic conservation laws Lany [17]

The extension of the approximate Riemann solver to three-dimensional is:

In the first step the flux vector  $F_{inv}$  evaluated with as  $u$  the normal velocity component, and  $v$  and  $w$  as the tangential components and the tangential components are passively convected by the normal component; but by taking the direction of flow of information in the normal direction into consideration.

Similarly the flux vector  $G_{inv}$  in  $y$ -direction is evaluated using  $v$  as the normal velocity component, and  $u$  and  $w$  as the tangential

components. Finally the flux vector  $H_{inv}$  in z direction is evaluated using  $w$  as the normal velocity component, and  $u$  and  $v$  as the tangential components Kopchenov and al [18]. The primitive variables are reconstructed to the left and right sides of the interface, using a 3rd order MUSCL scheme of Yamamoto and al [19] which is briefly outlined below.

$$U_{i+\frac{1}{2}L}^n = U_i^n + \frac{1-\varphi}{4} \Delta \bar{W}_{i+\frac{1}{2}}^n + \frac{1+\varphi}{4} \Delta \bar{W}_{i-\frac{1}{2}}^n \quad (11)$$

$$U_{i+\frac{1}{2}R}^n = U_{i+1}^n + \frac{1+\varphi}{4} \Delta \bar{W}_{i-\frac{1}{2}}^n + \frac{1-\varphi}{4} \Delta \bar{W}_{i+\frac{1}{2}}^n \quad (12)$$

$$\Delta W_{i+\frac{1}{2}}^n = W_{i+1}^n - W_i^n \quad (13)$$

$$\Delta W_{i-\frac{1}{2}}^n = W_i^n - W_{i-1}^n \quad (14)$$

$$\Delta \bar{W}_{i+\frac{1}{2}}^n = \text{minmod} \left( \Delta W_{i-\frac{1}{2}}^n, B * \Delta W_{i+\frac{1}{2}}^n \right) \quad (15)$$

$$\Delta \bar{W}_{i-\frac{1}{2}}^n = \text{minmod} \left( \Delta W_{i+\frac{1}{2}}^n, B * \Delta W_{i-\frac{1}{2}}^n \right) \quad (16)$$

The minmod flux limiter is defined as:

$$1 \leq B \leq \frac{(3-\varphi)}{(1-\varphi)} \quad (17)$$

$$\text{minimod}[x, y] = \text{sign}(x) \cdot \max[0, \min\{|x|, y \cdot \text{sign}(x)\}] \quad (18)$$

$$W = [\rho, u, v, w, p] \quad (19)$$

The solution was advanced in time using a two-stage explicit MacCormack [20]. This method is accurate, efficient and simple to implement on parallel computers and involves only two evaluations of the residual at each time step.

The stability of the time iteration method is dependent on the eigenvalues of the Jacobian matrices of the flux vectors and the properties of the time discretization method. To make sure not to take a too large time step the Courant-Friedrichs-Lewy (CFL) condition number and the von Neumann number (VNN) are used.

$$\Delta t_1 = \frac{CFL}{\max\left(\frac{|u|+c}{\Delta x}, \frac{|v|+c}{\Delta x}, \frac{|w|+c}{\Delta x}\right)} \quad (20)$$

$$\Delta t_2 = \frac{VNN}{\max\left(\frac{4\mu}{3\rho}, \frac{\gamma\mu}{\rho}, Pr\right) \left(\frac{1}{\Delta x^2}, \frac{1}{\Delta y^2}, \frac{1}{\Delta z^2}\right)} \quad (21)$$

$$\Delta t = \min(\Delta t_1, \Delta t_2) \quad (22)$$

## 4 Results and discussions

Let  $U_p$  and  $U_s$  are the velocities of the primary and secondary coaxial jet where velocity ratio is  $U_p/U_s = 0.7$  The Reynolds number based on the primary width jet is equal to  $Re = 62500$ . The computational mesh has  $385 \times 125 \times 125$  points. The physical domain of the computational extends to:  $45D_p \times 17D_p \times 17D_p$  in the axial direction, radial direction and tangential direction.

The time-averaged mean axial and radial velocities and their mean fluctuating values are calculated by time averaging the unsteady variables obtained from the LES results.

$$\langle \tilde{f} \rangle = \frac{1}{N_t} \sum_{n=1}^{N_t} \tilde{f}^n \quad (23)$$

$$\tilde{f}_{rms} = \sqrt{\frac{1}{N_t} \sum_{n=1}^{N_t} (\tilde{f}^n - \langle \tilde{f} \rangle)^2} \quad (24)$$

Where  $N_t$  represents the number of step.

In Figure 2, the average contours of the axial velocity in the (x, y) plane are shown. There is a clear distinction between the high velocity primary jet and the low velocity secondary jet, while downstream of the flow the radial velocity gradients become smaller.

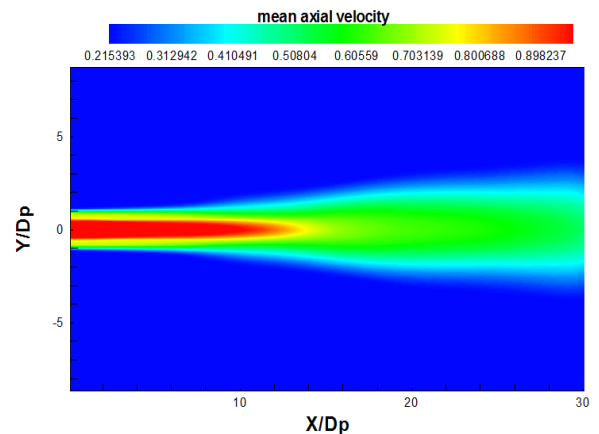
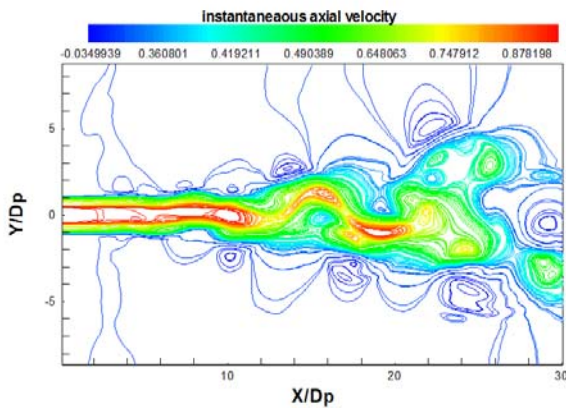


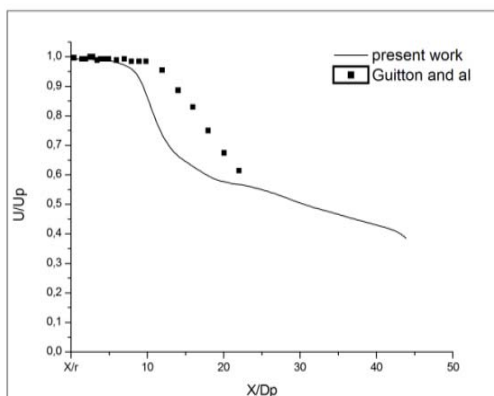
Fig. 2. Mean axial velocity



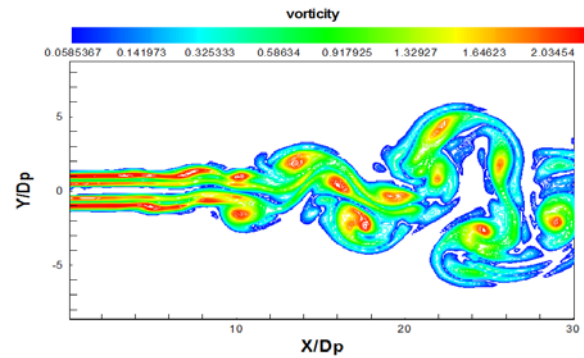
**Fig. 3 cut through the plane (x, y) of the instantaneous fields of the longitudinal velocity**

Figure 3. Show a cut through the plane (x, y) of the instantaneous fields of the axial velocity. Instabilities are observed to develop and expand in the near field of the primary jet nozzle. Macrostructures form in the inner mixing layer and separate from the flow, and end of the central core potential. Other large structures form around the secondary jet, detach further downstream and interact with the developed region of the primary jet.

The decay of the axial velocity along the coaxial jet axis of our simulation is shown in Fig. 4. The length core potential is defined as the average axial velocity decreased to 95% of the coaxial jet velocity at  $y = 0$ . We see the good agreement between our results and experimental results Guitton and al [21].



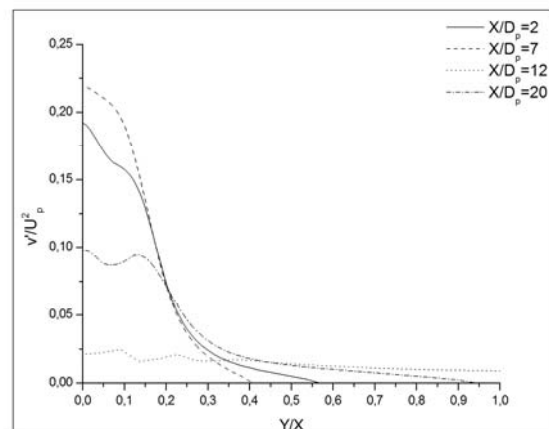
**Fig.4. the decay of the longitudinal velocity along the coaxial jet axis**



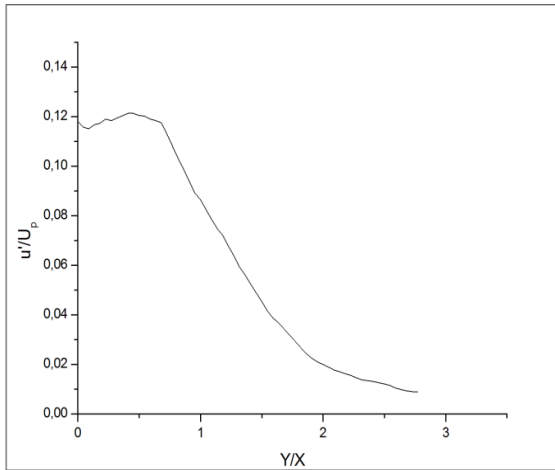
**Fig.5. cut through the plane (x, y) of the vorticity field**

Figure 5 show a cut through the plane (x, y) of the vorticity field. It is observed how the shear layer instabilities develop in the direction of the overall flow as well as the fully developed turbulence downstream of the flow. This process is as follows: firstly, the small perturbations develop independently in the two shear layers (internal and external), leading to a winding of the layers and vortex pairings.

Figure 6-7 gives the profiles of radial and axial fluctuations velocity component as function of the radial direction. It is observed that in the initial zone, the turbulence production is localized in the regions where the highest average velocity gradients prevail. In the intermediate zone of the flow, the turbulence peaks spread out and the end of the potential zone is marked by the increase of the level of turbulence. The mixing layers interacted and merged into a turbulence zone developed downstream of their junction on the axis coaxial jet.



**Fig.6. rms radial velocity profile at different positions**



**Fig.7. rms axial velocity profile**

The amplitude of the fluctuation components of the velocity gives information on the nature of the instabilities developing in the shear regions. A higher value of the axial component  $\hat{u}$  with respect to the  $\hat{v}$  component in outer shear is typical of the free shear layers. The wake effect observed in the inner shear zone, as the radial velocity fluctuations  $\hat{v}$  is larger amplitude. Wake Instabilitie dominated in the inner shear zone a short distance downstream of the flow.

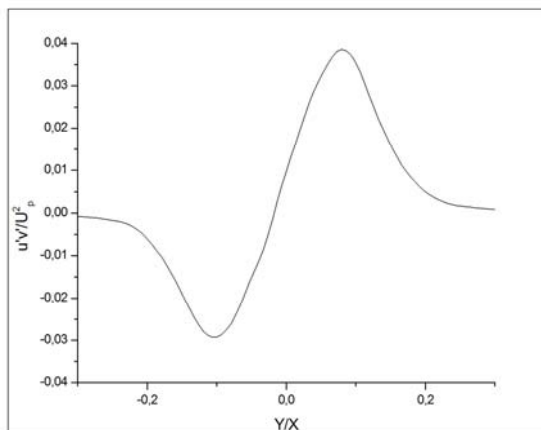


**Fig.8. shear stress Reynolds  $\hat{u}\hat{v}$**

Figure.8. show a plot of the shear stress Reynolds  $\hat{u}\hat{v}$  as a function of the radial coordinate. Profiles confirm the presence of wake instability, as the shear stress Reynolds, of sign opposite. The average velocity gradients, indicates the presence of vortex structures having opposite directions of rotation. The expansion and interaction of these structures with the downstream distance is confirmed by the widening and the decrease the profile of  $\hat{u}\hat{v}$ .

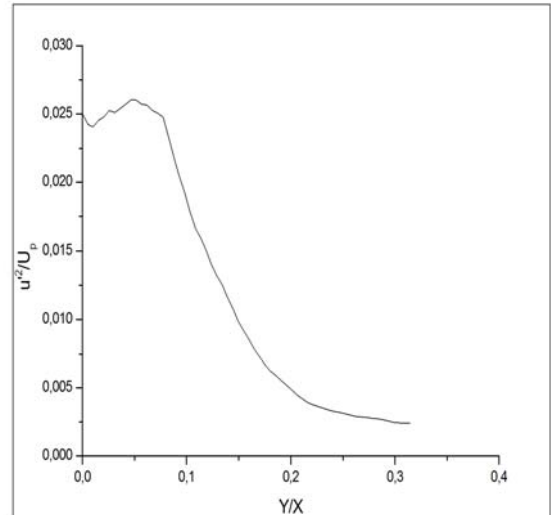


**Fig.9. axial intensité turbulent profile  $\hat{u}^2$**

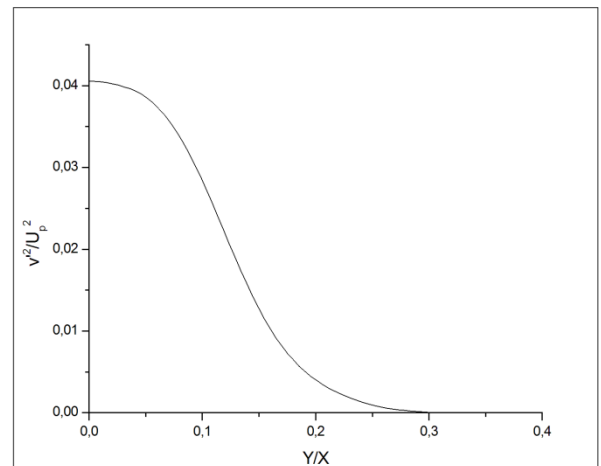


**Fig.10. radial intensité turbulent profile  $\hat{v}^2$**

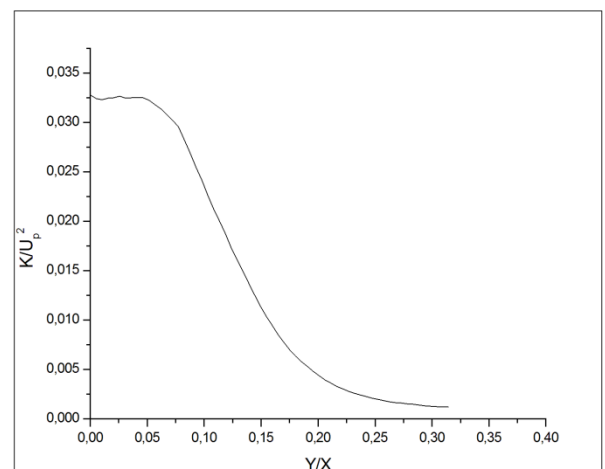


**Fig.11. kinetic energy turbulent**

The distribution of turbulent intensities is closely related to the shape of the average input velocity

profile. The drop in velocity in the primary core potential is due to the internal fluid training in the inner mixing layer. The large vortex structures that develop in the inner mixing layer are mainly responsible for this training. To further illustrate the disturbance development of our simulation. The distribution of the axial, radial turbulent intensity and the turbulent kinetic energy in the fully developed zone are plotted in Figs. 9-11 as a function of the radial coordinate. We can see the achievement of the state of the self-similarity of the flow, which shows the good quality of the result. There is a strong transfer of momentum from the primary jet towards the secondary jet. The level of turbulent intensity remains significant throughout the width of the jet, this due to the longitudinal structures of turbulence.

The rate of fluctuation of the longitudinal velocity on the axis of the primary jets is shown in Fig. 12., the growth of the turbulence intensity on the primary jet axis is more and more up to  $x/D_p = 6x$ , the peak of maximum amplitude of turbulent intensity is reached when the inner and outer shear layers merge, downstream of the core potential of the primary jet. Our results are generally in agreement with the experimental data. As observed by Bogey and Bailly [19].

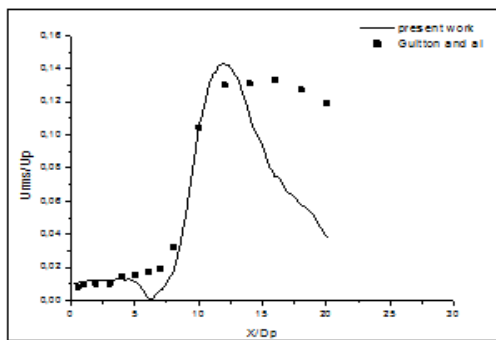


**Fig. 12. rms axial velocity profile in axial direction**

To visualize the vortex structures as a function of the frequency, it is necessary to analyze the power spectral density of the radial velocity fluctuation as a function of the Strouhal number.

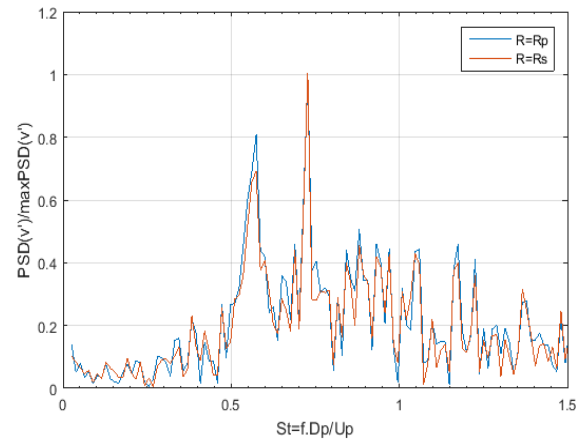


**Fig.13. PSD radial velocity profile**

the spectral power density (PSD) of the Unsteady fields of radial velocity, is shown in Figure 7, this figure gives the PSD as function of the number of Strouhal  $St = \frac{f U_p}{D_p}$ , evaluated at the region of fully developed turbulence along the  $R = R_p$  and  $R = R_s$ , in  $\frac{x}{D_p} = 4$  we observe the predominance of an axis-symmetric mode on each of the shear layers. This mode is characterized by Strouhal number peaks  $St = 0.6$  in inner shear and  $St = 0.7$  for the outer layer.

Figures 7-8 show the plots of the power spectral density of unsteady fields of axial velocity, and temperature in the fully developed zone. The spectrum of the unsteady velocity takes the law of theoretical power in  $k=-5/3$  in the inertial zone.

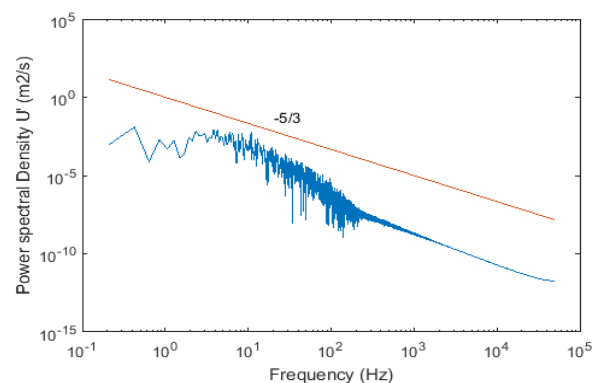


**Fig.14. PSD unsteady fields of axial velocity**

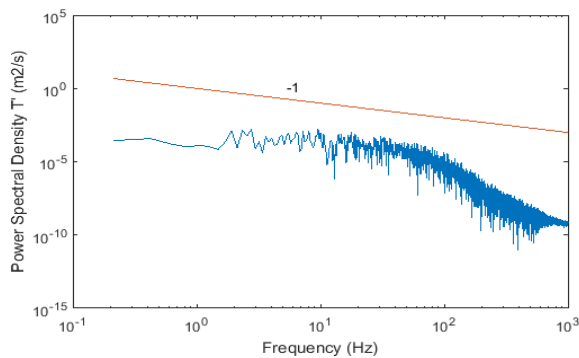


**Fig.15. PSD of temperature fields**

The plot of the power spectral density of the temperature in inertial zone having a power law in  $k=-1$ . The temperature behaves here like a passive scalar, and the law of power  $-1$  confirm to its intermittent nature. Finding power laws in  $k=-5/3$  for the velocity spectrum and  $k=-1$  for the temperature spectrum, clearly validates the good behavior of the LES model, and these results confirm that coaxial jets can be like to single jets in the fully developed zone.

## Conclusion

In this work we study a compressible, and turbulent coaxial jet by a numerical approach of the Large Eddy Simulation. The main research, of this study was based on the implementation of the modern numerical methods. Adapted to the turbulent compressible flow as coaxial jet, and making it possible, to answer the requirements in terms of precision of the results and cost of computation. The main results obtained in this study are: In the initial development zone of the flow, the turbulence production is localized in areas with the highest average velocity gradients. In the intermediate zone of the flow, the turbulence peaks spread out and the end of the potential zone is marked by the increase of the level of turbulence. Mixing layers interacted and merged into a turbulence zone developed downstream of their junction, on the axis of coaxial jet. The profiles of the shear stress Reynolds confirm the presence of wake instability in the flow. The disturbances of the PSD of the unsteady axial velocity fields as function of the number of strouhal. We observe the predominance of an axis-symmetric mode on each of the shear layers. This mode is characterized by Strouhal number peaks  $St = 0.6$  in inner shear and  $St = 0.7$  for the outer layer. Finding power laws in

$k=-5/3$  for the velocity spectrum and  $k=-1$  for the temperature spectrum, clearly validates the good behavior of the use LES model in our simulation.

## References:

- [1] N. W. M. Ko and A. S. H. Kwan. The initial region of subsonic coaxial jets. *J. Fluid Mech.*, 73 :305–332, 1976.
- [2] F. H. Champagne and I. J. Wygnanski. An experimental investigation of coaxial turbulent jets. *Int. J. Heat Mass Transfer*, 14 :1445–1464, 1971.
- [3] W. Forstall and A. H. Shapiro. Momentum and mass transfer in coaxial gas jets. *J. Applied Mech.*, 17 :399–408, 1950.
- [4] M. Favre-Marinet and E.B. Camano Schettini. The density field of coaxial jets with large velocity ratio and large density differences. *Int. J. Heat and Fluid Flow*, 44 :1913–1924, 2001.
- [5] M. Favre-Marinet, E.B. Camano Schettini, and J. Sarboch. Near-field of coaxial jets with large large density differences. *Exp. Fluids*, 26 :97–106, 1999.
- [6] T. J. Williams, M. R. M. H. Ali, and J. S. Anderson. Noise and flow characteristics of coaxial jets. *J. Mech. Engng Sci*, 2 :133–141, 1969.
- [7] D. S. Dosanjh, J. C. Yu, and A. N. Abdelhamid. Reduction of noise from supersonic jet flows. *AIAA Journal*, 9 :2346–2353, 1971.
- [8] A. S. H. Kwan and N. W. M. Ko. The initial region of subsonic coaxial jets. Part II. *J. Fluid Mech.*, 82 :273–287, 1977.
- [9] W. J. A. Dahm, C. E. Frieler, and G. Tryggvason. Vortex structure and dynamics in the near field of a coaxial jet. *J. Fluid Mech.*, 241 :371–402, 1992.
- [10] R. B. Wicker and J. K. Eaton. Near-field of a coaxial jet with and without axial excitation. *AIAA Journal*, 32 :542–546, 1994.

- [11] H. Au and N. W. M. Ko. Coaxial jets of different mean velocity ratios. *J. Sound Vib.*, 116 :427–443, 1987.
- [12] P. G. Gladnick, A. C. Enotiadis, J. C. Larue, and G. S. Samuelsen. Near-field characteristics of a turbulent coflowing jet. *AIAA Journal*, 28 :1405–1414, 1990.
- [13] E. B. Camano-Schettini. Etude expérimentale des jets coaxiaux avec différences de densité. PhD thesis Institut National Polytechnique de Grenoble, 1996.
- [14] T. S. Zawacki and H. Weinstein. Experimental investigation of turbulence in the mixing region between coaxial streams., 1968. NASA Contractor Report CR-959.
- [15] H. Rehab, E. Villermaux, and E. J. Hopfinger. Flow regimes of large-velocity-ratio coaxial jets. *J. Fluid Mech.*, 345 :357–381, 1997.
- [16] H. Rehab. Structure de l'écoulement et mélange dans le champ proche des jets coaxiaux. PhD thesis Institut National Polytechnique de Grenoble, 1997.
- [17] C.B. Laney, *Computational Gas Dynamics*, Cambridge University Press, 1993.
- [18] V. I. Kopchenov, A. N. Kraiko, A second-order monotone difference scheme for hyperbolic systems with two independent variables, *U.S.S.R. Comput. Math. Math. Phys.*, **23**:4 (1983), 50–56
- [19] S. Yamamoto, H. Daiguji, Higher order accurate upwind schemes for solving compressible Euler and Navier–Stokes equations, *Comput. Fluids* 22(2/3) (1993) 259–270.
- [20] MacCormack, R.W. 1969, The Effect of Viscosity in Hyper Velocity Impact Cratering, *Journal of Space Craft* 69-354.
- [21] A. Guitton. Etude expérimentale des relations entre les champs hydrodynamiques et acoustiques des jets libres. Thèse de Doctorat, Université de Poitiers (2009).
- [22] C. Bogey, S. Barré, P. Juve, and C. Bailly, Simulation of a hot coaxial jet : Direct noise prediction and flow-acoustics correlations, *Physics of Fluids* 21 (2009).